Engineering Structures 132 (2017) 609–623

Contents lists available at ScienceDirect

Engineering Structures

journal homepage: www.elsevier.com/locate/engstruct

Review of experimental cyclic tests on unreinforced and strengthened masonry spandrels and numerical modelling of their cyclic behaviour

G. Rinaldin *, C. Amadio, N. Gattesco

University of Trieste, Department of Engineering and Architecture, Piazzale Europa 1, 34127 Trieste (TS), Italy

ARTICLE INFO

Article history:
Received 14 December 2015
Revised 26 November 2016
Accepted 28 November 2016

Keywords:
Non-linear modelling
Masonry spandrel
Cyclic behaviour
Mechanical model
Strengthening techniques

ABSTRACT

A reliable numerical modelling for the cyclic behaviour of unreinforced and strengthened masonry spandrels is herein presented. The proposed numerical model is adapted from Tomazevic-Lutman's model for masonry piers in shear and it has been validated upon an experimental campaign conducted at Department of Engineering and Architecture of University of Trieste. The tests were conducted on H-shaped full-scale specimens imposing vertical displacements of increasing amplitude on one leg. Four unreinforced masonry specimens arranged with different masonry material (bricks and stones) and lintel supports (wooden lintel, masonry arch) were considered. Each specimen was then reinforced with a different strengthening technique (tensioned bars, steel profiles, CFRP laminates) and re-tested. Analytical relationships were proposed, based on those available in some Codes of Practice, to estimate the maximum shear resistance of URM and RM spandrels. These relationships provide resistance values in good agreement with the experimental results and can be correctly employed to define the cyclic model of the spandrel to be used in the numerical simulation. The cyclic shear-displacement curves obtained through the numerical model are in good agreement with those of the experimental tests and very good assessment of the dissipated energy was obtained.

1. Introduction

Unreinforced masonry (URM) buildings represent a large portion of existing structures in most earthquake prone regions. The evaluation of the seismic vulnerability of these buildings is of actual importance. In fact, these buildings have shown poor performance in past earthquakes causing heavy damage, structural collapse and casualties [1,2]. Due to both the frequent location of these types of structures in areas characterized by medium to high seismic hazard and their low shear capacity to seismic excitation, it is required to perform the structural assessment and to provide the most useful intervention in order to adequately improve the structural performances of these buildings when subjected to earthquakes.

A good knowledge of the building is needed to develop a reliable assessment of the capacity and to detect their structural shortcomings. The built heritage, in fact, is characterised by a wide range of construction techniques used for both walls and floors. Many different materials are normally used for masonry walls (e.g. solid bricks, stone blocks, rubble stones, cobblestones, etc.) and arranged with various textures (single leaf or multiple leaves with or without diatones, coursed blocks or uncoursed stones, etc.). The floors are mostly wooden made, but also masonry vaults and precast beams with ceiling bricks can be found.

In the case of perforated walls, the behaviour is strongly influenced by the coupling between piers and spandrels. In fact, in case of horizontal loads applied to a perforated wall, the spandrel element affects both strength degradation and lateral resistance of the wall. If there are weak piers and strong spandrels, the damage is mostly concentrated in the piers, but in case of strong piers and weak spandrels the wall performance is strongly dependent of the spandrel response. Some recent experimental studies proved that in many cases the spandrel provides a very important resistance contribute to the masonry wall shear capacity (e.g. [3–9]).

A rough knowledge of the structural system in conjunction with an inadequate analysis may lead to either overestimate or underestimate the safety of these structures. In the first case serious risks for human lives can be met, while a large increment of costs may be due to the excessive strengthening measures related to the latter case. Furthermore, an underestimation of the building capacity may request strengthening interventions with important changes in the original structures.

In the professional practice, due to the high costs connected to a rigorous evaluation, the analyst usually choose the most suitable

* Corresponding author.
E-mail addresses: grinaldin@units.it (G. Rinaldin), amadio@units.it (C. Amadio), gattesco@units.it (N. Gattesco).

http://dx.doi.org/10.1016/j.engstruct.2016.11.063
0141-0296/

schematization for the masonry wall between the "weak spandrel-strong pier" type and the "strong spandrel-weak pier" type, as suggested by the "Prestandard for the Seismic Rehabilitation of Existing Structures" [10]. Both approaches are formulated on the bases of simplified assumptions concerning the capacity of spandrels. In the first case, the strength of spandrels is neglected and the horizontal forces are supported only by the piers, which span from the foundation to the roof of the building. In the latter case, the spandrels are assumed to be infinitely stiff and resistant, thus a shear type behaviour is assumed for the piers and the building collapse is associated to a storey mechanism. Because of these strong assumptions on the masonry spandrel behaviour, both approaches provide a rough estimation of the actual deformability and capacity of perforated masonry shear walls.

The definition of reliable analytical and numerical models for the seismic evaluation of URM buildings has been the object of several studies in the last two decades. Depending on the field of use, various models concerning different theoretical approaches have been developed. Many of such models are used for research and, being based on complex finite element formulations (e.g. [11]), they are high computation demanding, so that they cannot be employed for realistic analyses of whole buildings.

Many other different models have been developed for the analysis of URM structures; most of them use one-dimensional macro-elements to model the masonry wall so the seismic performance of whole buildings can be assessed with an acceptable computational effort. In particular, in last nineties, improved numerical models based on the equivalent frame approach have been defined. In these models, suggested by the current design codes of practice (e.g. [12,10]), different failure mechanisms (i.e. shear with diagonal cracking, shear with sliding and rocking) are provided for each macro-element (as in [13–15]). Chen et al. [16] proposed an interesting practical approach that allows analysing the in-plane behaviour of unreinforced masonry perforated walls, within an equivalent frame model taking into account different types of failure modes. A particular macro-element allows modelling piers and spandrels; the formulation of this macro-element includes three nonlinear shear springs in series with two rotational springs and an axial spring in order to simulate axial failure, bed joint sliding, diagonal tension, rocking collapse and toe crushing. The validation of the model was given only for piers because of the lack of experimental test on spandrels.

Such numerical models have been developed on the basis of both theoretical and experimental results. But, while many experimental outcomes (shear-compression test, diagonal compression test, etc.) on numerous types of masonry, even under cyclic loads are available for piers, to date very little tests have been carried out on the behaviour of spandrels. These experimental achievements are of paramount importance because the spandrel structural response is considerably different from that of the piers. In fact, under seismic loads, the masonry beams are subjected to shear and bending with negligible axial force.

It is necessary to analyse the available strengthening techniques so to evidence their effectiveness to increase the bending and shear resistance of spandrels. The most frequently utilized strengthening techniques are the application of pre-tensioned tie-rods, the gluing of CFRP strips on both faces of the masonry or the coupling of RC tie-beams.

To study the above mentioned problems, in recent years several studies has been carried out. Based on the earthquake damage observations, Cattari and Lagomarsino [17] reduced the possible failure mechanisms for spandrels without coupled reinforced concrete beams or tie-rods, to the most frequent: diagonal cracking or rocking. Through a preliminary theoretical study on brick walls, they underlined that the interlocking phenomena at the interface between spandrel ends and contiguous masonry provide significant flexural resistance to the spandrel, even in absence of tension-resistant elements. On this concern, some predictions are reported also in FEMA 306 [18].

A first reliable experimental study for the cyclic behaviour of spandrel was presented by Gattesco et al. [3]. The test set up was made by a full-scale specimen composed by two piers connected by a spandrel, so the sample have an H shape. Then, one of the piers was forced to move vertically with a cyclic load history so to simulate the stress condition in the spandrel occurring in a perforated wall subjected to in-plane horizontal cyclic forces, as for earthquake excitation.

Each specimen was tested, in a first time, as unreinforced and then the sample was strengthened with the application of a reinforcing technique. Thus, the strengthened sample was subjected to the cyclic test again and the results evidenced the effectiveness of the intervention.

A similar test set up was recently adopted also at the University of Pavia by Graziotti et al. [19] to perform two experimental tests on stone spandrel specimens: the first sample was tested without any reinforcement, while in the second test an axial force was applied to the spandrel so to simulate the effects of a tie-rod. A slightly different test methodology was proposed by Beyer and Dazio [5]: instead to move vertically one pier with respect to the other, both piers are rotated at their base. The effects of a varying axial force on the spandrel force-deformation characteristics were also investigated by means of rods that were pre-tensioned and locked-in. Four brick masonry spandrels were studied: two were made with a wooden lintel and two with a shallow masonry arch.

In the paper, the results of an experimental campaign developed after a first investigation carried out at the University of Trieste [3,20] are presented and discussed. In particular, four H shape specimens, three made of brick masonry and one of rubble stone were analysed before and after the application of different reinforcement techniques on the spandrel. Interesting results, both in terms of resistance and deformability of the spandrel, were obtained.

Besides, in order to modelling the hysteretic behaviour of spandrels, a cyclic model is proposed and implemented in the FE code ABAQUS. The proposed model can be used in the ambit of the equivalent frame method; every single spandrel is composed by an assemblage of rigid links and zero-length springs. The nonlinear spandrel model, implementing stiffness and strength degradations, can be easily used in static and dynamic non-linear analyses.

2. Experimental tests

Eight experimental tests were carried out on full scale masonry specimens, representing a portion of a perforated wall. The test apparatus was studied in order to subject the spandrel to a loading condition that simulates the actual state of stresses occurring in the perforated walls in case of in-plane horizontal forces.

In particular, three unreinforced samples made of clay brick masonry and one made of rubble stone were built. After the cyclic test on the plain sample, stopped just before the collapse so as to allow applying the strengthening technique, each specimen was tested again in order to evaluate the effects of the reinforcement on the spandrel performance. The effectiveness of three intervention techniques were investigated on the brick masonry samples: the application of a couple of horizontal steel ties, the application of one L-shaped steel profile to the internal face of the wall at the floor level and the gluing of CFRP (carbon fibre-reinforced polymer) horizontal laminates on both surfaces. The sample made of stone was strengthened with the coupling of an L-shape steel profile on the internal surface of the wall. In this way, it was possible

to compare the effectiveness of the same strengthening technique applied on different masonry types.

The test samples are formed by two piers connected at their mid-height by a spandrel, as to form an H-shape specimen. In order to simulate a portion of a perforated wall, the piers length is equal to the distance between the mid-height of two consecutive floors of a representative building (Fig. 1a). During the test, one pier is fixed at the base of the laboratory, while the other is forced to translate up and down without any rotation for the faces at the base and at the summit of the piers (Fig. 1b).

The first three tested specimens are made with alternating stretching and heading courses of clay bricks and have a thickness equal to one and a half brick (380 mm). The bricks in each masonry layers are placed as commonly used in ancient buildings. In the first specimen (MS1), at the bottom of the spandrel a wooden lintel with the same width of the wall and depth equal to 120 mm was placed. The second and the third specimens (MS2 and MS3 respectively) are similar (dimensions in Fig. 2a); in both samples a flat arch (250 mm thick) and a wooden lintel (120 mm) are set at the bottom of the spandrel. The latter sample (MS4) is made of rubble stones arranged to form a wall with 400 mm of thickness and a wooden lintel is set in the spandrel with a width equal to the thickness of the wall and depth equal to 120 mm (dimensions in Fig. 2b).

As aforesaid, the cyclic test on the unreinforced samples was stopped just before the collapse and the specimens were recomposed closing the cracks and strengthened. Then the reinforced walls were loaded up to failure level.

Hence, the MS1r sample is the first tested wall reinforced with a couple of horizontal steel ties arranged as shown in Fig. 3a. The MS2r sample was obtained strengthening the MS2 specimen by applying a L-shaped steel profile ($100 \times 150 \times 15$ mm) clamped to the internal face of the wall at the floor level by means of injected dowels (d = 16 mm). These devices were driven into the wall with 500 mm spacing and injected with epoxy resin (Fig. 3b). This angle beam simulates the presence of a border element used to improve the connection and the stiffness of the wooden floor to the masonry (e.g. [21]).

The spandrel of the MS3 sample was reinforced (MS3r) by gluing at the top and at the bottom of the element CFRP laminates, at both sides of the wall (Fig. 3c). Finally, The MS4r test was carried out on the MS4 specimen reinforced with the application of an L-shaped steel profile on one side of the wall, as for the MS2r sample.

Specific tests were carried out on samples to determine the mechanical characteristics of the materials used in the experimental campaign. In particular, simple tests on masonry triplets have been performed to determine the initial shear strength under zero compressive stress in mortar joint direction (cohesion) of the masonry. This has been done for MS1, MS2 and MS3 specimens, while for the stone spandrel the shear strength was obtained through diagonal compression tests [22,23]. The characteristics are summarized in Table 1.

The specimens described in the previous section were built and tested in the Laboratory for Testing Materials and Structures of the University of Trieste. The air curing procedure was about 60 days since the completion of the specimen construction. As shown in Fig. 4, the pier on the left was fixed to the stiff concrete base of the Laboratory while the pier on the right side, during construction and curing, was laid on provisional supports. A stiff steel element was placed on the top of the right pier and was connected to its bottom by means of six vertical Dywidag steel bars. These bars, applied also on the left pier, allowed to enforce a compressive stress to the vertical masonry elements in order to simulate the effects of gravity loads that normally act on the wall (e.g. self-weight, floor reactions). In all the eight tests, the Dywidag bars were tensed to obtain on both piers an average compressive stress equal to 0.5 MPa. This value of axial stress corresponds to a common value that can be found in a three-story residential masonry building. The axial force in piers has not been controlled during the tests.

Test setup was already described in deep in [7] and is omitted here. Fig. 4 reports the 4 test setups from an angle realized for the unreinforced specimens.

The test was continued in unreinforced specimens up to reaching a maximum vertical displacement of about ±8 mm (equal to 1/125 of the spandrel length), so as to obtain a severe damage but not the collapse. In strengthened specimens the samples were loaded up to failure level.

2.1. Experimental results

The global response of the spandrels in a masonry perforated wall may be summarized by the relationship between the shear load applied on the spandrel and the relative vertical displacement surveyed at the spandrel end.

The total vertical displacement of the spandrel is then corrected in order to consider the rotation of the piers at the spandrel intersection, which is obtained on the basis of the rotations measured by the inclinometers positioned on the piers.

In Fig. 5a the relationship between the shear load and the vertical displacement of the spandrel of the MS1 specimen is shown. The behaviour of the element is almost the same in both loading directions with a maximum shear capacity of about 70 kN. After the peak load, a gradual decrease in shear capacity was observed. In correspondence of the end of the test, a residual strength of about 30 kN was surveyed, equal to approximately 40% of the peak resistance. The ultimate transversal displacement was about five times greater than that corresponding to the peak load (10 mm corresponding to 1% drift).

At the end of the test, sub vertical cracks were observed in correspondence of the ends of the spandrels. After this test, the vertical cracks were closed through the application of a couple of steel ties. In particular, these devices were two Dywidag bars with a diameter of 27 mm and they allowed impressing a compressive horizontal force to the spandrel stabilized to 64 kN. A second test was carried out on this reinforced sample (MS1r). The obtained load – displacement relationship is displayed in Fig. 5b: a maximum shear resistance of about 95 kN was obtained in both directions. After the peak, a progressive reduction in the resistance was observed. In correspondence of a drift equal to 6% (5 times the displacement observed at the maximum resistance) the residual strength was about 60–70% of the maximum. The comparison of the relationships of the MS1 and MS1r samples, shown in Fig. 5b, allows observing an increment both in terms of maximum shear resistance (about 35% with respect to the plain sample) and in terms of ultimate displacement (6 times the displacement observed for the URM specimen). For both tests, there was no direct control of the axial force in the spandrel during the test.

In Fig. 6a the shear load against the vertical displacement of the spandrel of the MS2 specimen is displayed. The peak load is about 50 kN in both loading directions; the decrease of resistance is appreciable just after the peak, and a residual strength of about 40% of the maximum was maintained up to the end of the test. The test was stopped in correspondence of a displacement equal to about 1% of the spandrel length (10 mm). In this case, shear cracks were observed at the end of the test (diagonal cracks).

Then, the specimen was repaired as made for MS1 and strengthened coupling an L-shaped steel profile to the wall through 16 mm driven dowels. The test carried out on this sample (MS2r) allowed obtaining the load – displacement relationship plotted in Fig. 6b. The comparison with the results of the URM sample highlighted an increment in the maximum shear resistance of about 30% (equal

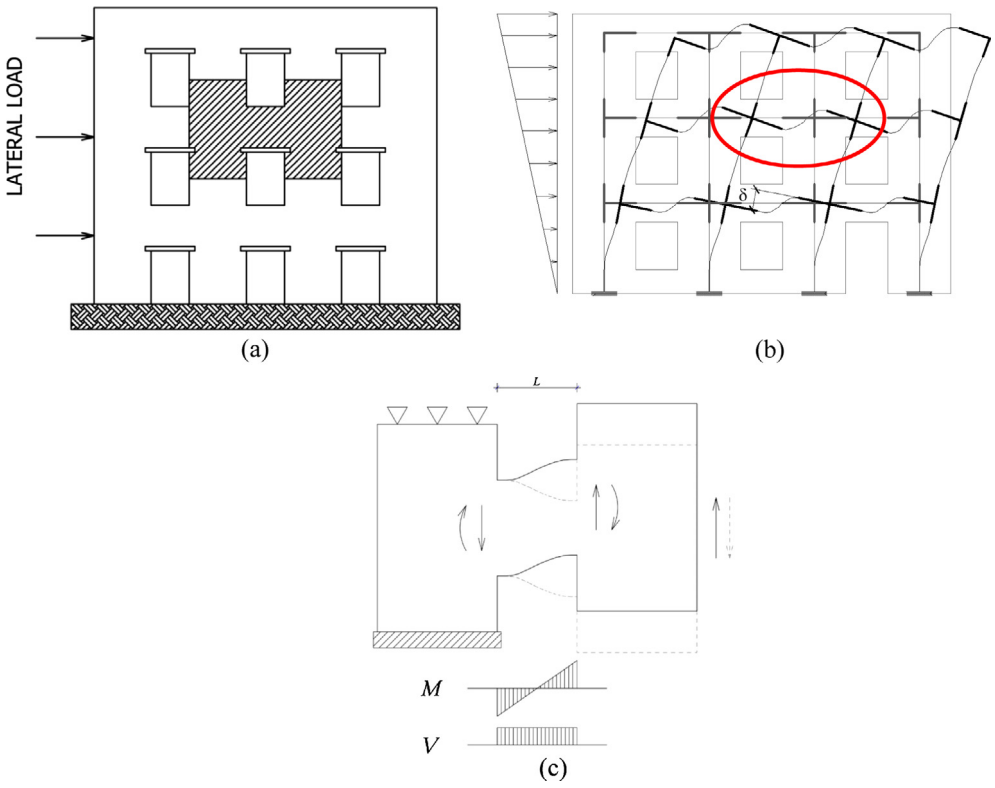

Fig. 1. (a) Masonry perforated wall; (b) deformation of spandrels due to horizontal action; (c) experimental model of the test.

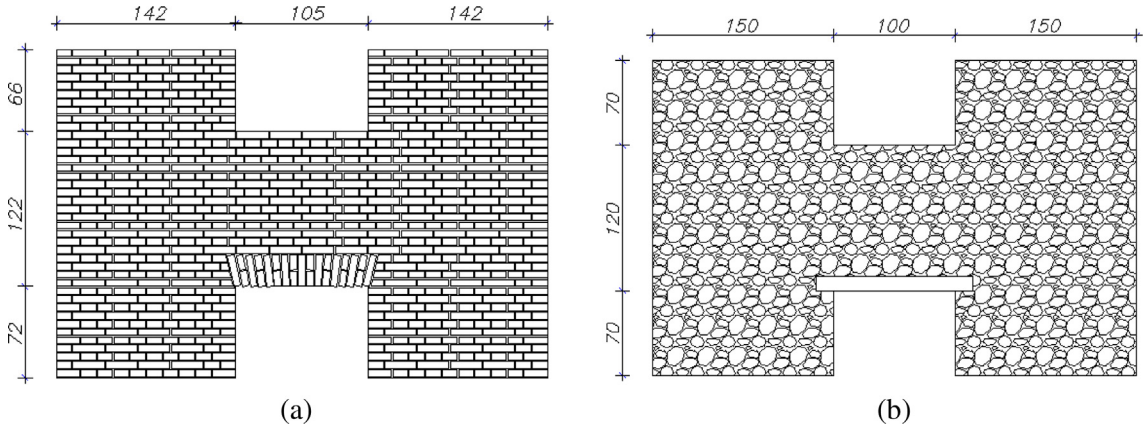

Fig. 2. (a) Specimen with a flat arch (MS2); (b) stone specimen (MS4).

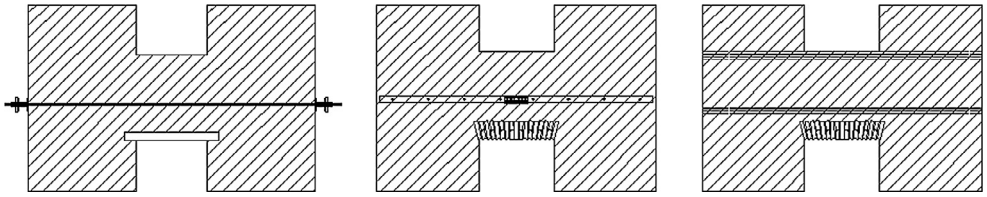

Fig. 3. Spandrel specimen reinforced with steel ties (left, a), with steel beam (centre, b) and with CFRP laminates (right, c).

to about 65 kN in both directions), while the ultimate displacement was amplified almost 6 times, reaching a spandrel drift of about 6%.

As stated, the MS3 sample is equal to MS2. After the test on the plain specimen, the cracks of the spandrel were closed. In particular, a stabilized horizontal compressive stress of 0.15 MPa was applied to the spandrel using a couple of horizontal steel ties (two Dywidag bars 27 mm diameter). Then the specimen was reinforced gluing on both surfaces of the wall a couple of CFRP laminates (four CFRP laminates, 120 × 1 mm), placed at the top and

Table 1
Mechanical characteristics of materials employed in the tests.

Mechanical characteristic	MS1/MS1r [MPa]	MS2/MS2r [MPa]	MS3/MS3r [MPa]	MS4/MS4r [MPa]
Mortar joint compressive strength	2.17	2.48	2.08	2.25
Brick compressive strength	44	44	47	–
Brick dimensions/stones diameter	55 × 120 × 250 mm	55 × 120 × 250 mm	55 × 120 × 250 mm	400 mm
Mortar joints compressive strength	2.17	2.48	2.12	2.12
Masonry horizontal compressive strength	7	7	6.8	3.6
Shear strength with no compression from triplet tests	0.19	0.22	0.22	
Masonry shear strength from diagonal compr. test				0.1
Yielding stress/tensile strength of Dywidag bars	950/1050			
Yielding stress/tensile strength of threaded dowels		480/590		480/590
Yielding stress/tensile strength of angle profile		324/455		324/455
Composite laminate tensile strength (fibres direction)			2850	
Composite laminate Young modulus (fibres direction)			175,000	
Composite laminate shear strength (perp. to fibres)			95	

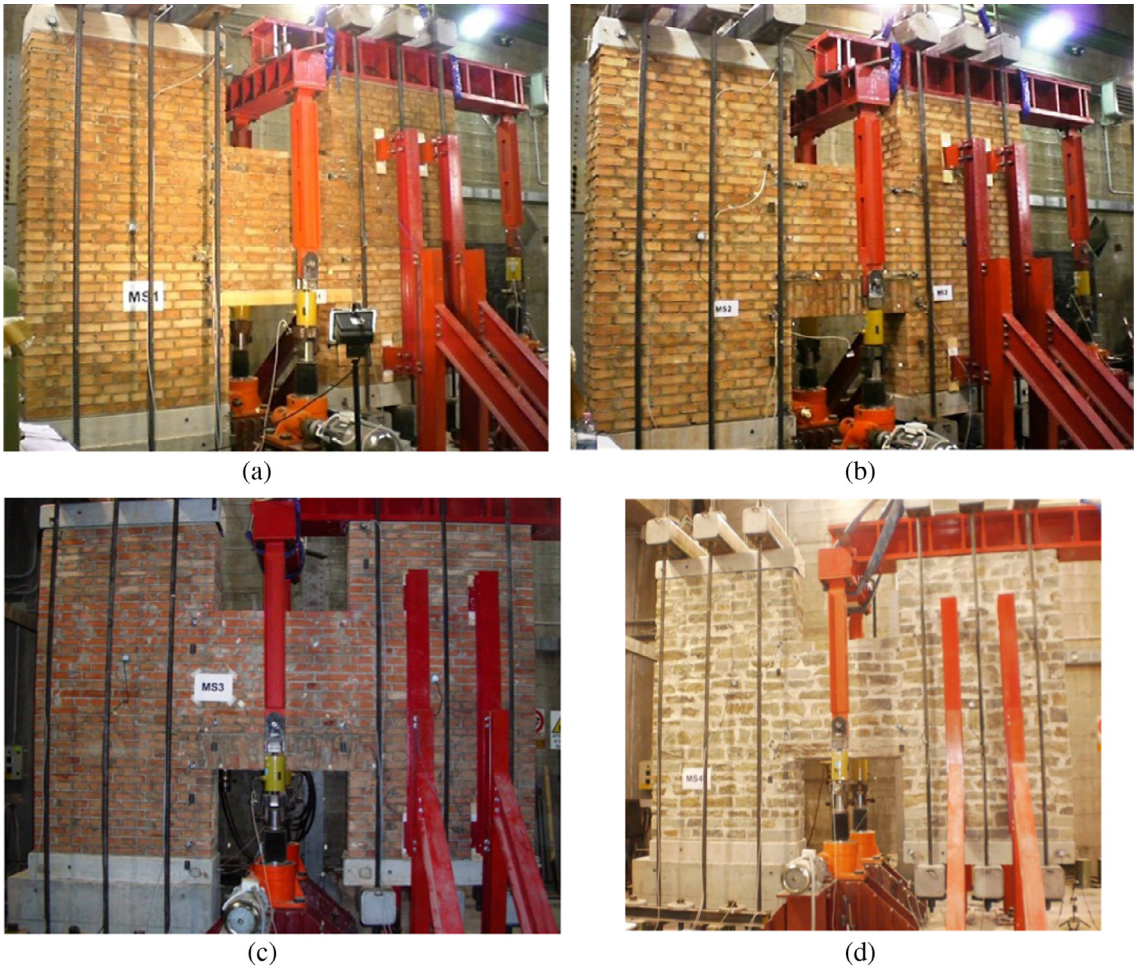

Fig. 4. Pictures of the four test setups for unreinforced specimens: MS1 (a), MS2 (b), MS3 (c), MS4 (d).

the bottom of the spandrel. Finally, the steel bars were removed and the axial force in the spandrel was not monitored during test.

As in the test on the MS2 sample, the main cracks on MS3 spandrel were diagonal (shear cracks). The unreinforced test showed diagonal cracking quite early [20]. The relationship between the shear load and the transversal displacement of this specimen is plotted in Fig. 7a. The maximum shear resistance surveyed during the test was about 45 kN, in both loading directions. After the peak, the shear strength reduced to 40–50% of the maximum shear, at a displacement equal to 0.8% of the spandrel length.

The response in terms of shear load against the relative vertical displacement of the reinforced specimen MS3r is plotted in Fig. 7b ([1]red line), while the black curve is that obtained in unreinforced tests. The maximum resistance reached in the test is almost three times the resistance achieved with the unreinforced specimen (about 130 kN). After the peak of resistance, the behaviour is different for

[1] For interpretation of color in Figs. 5, 6, 7 and 8, the reader is referred to the web version of this article.

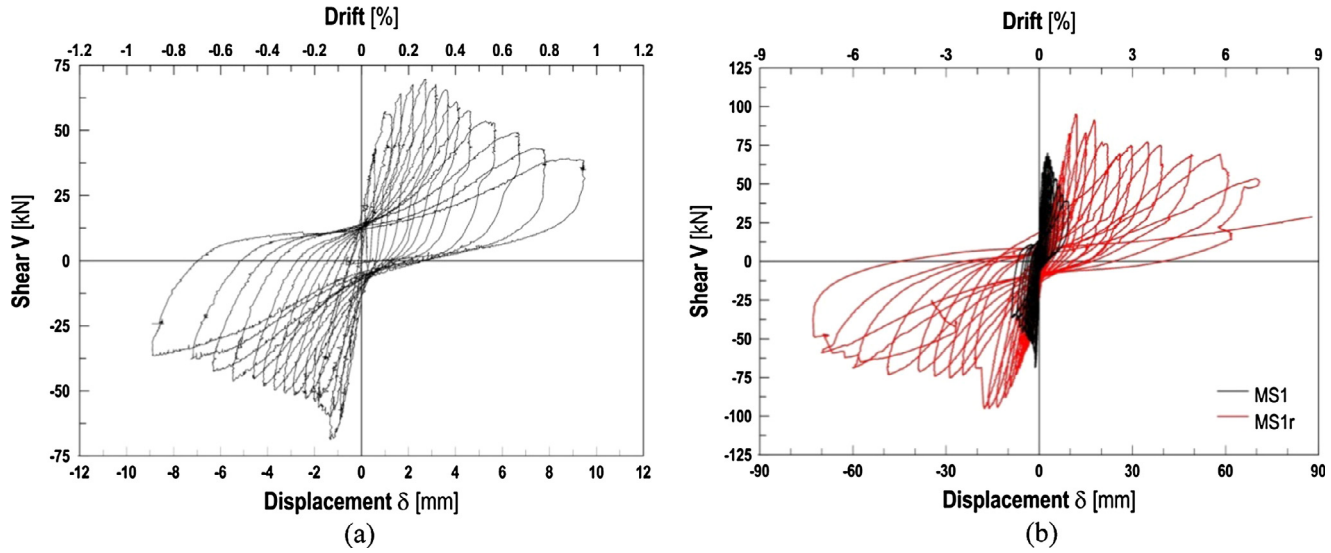

Fig. 5. MS1: shear load against vertical displacement (a); comparison of the behaviour of URM specimen MS1 and RM specimen MS1r (b).

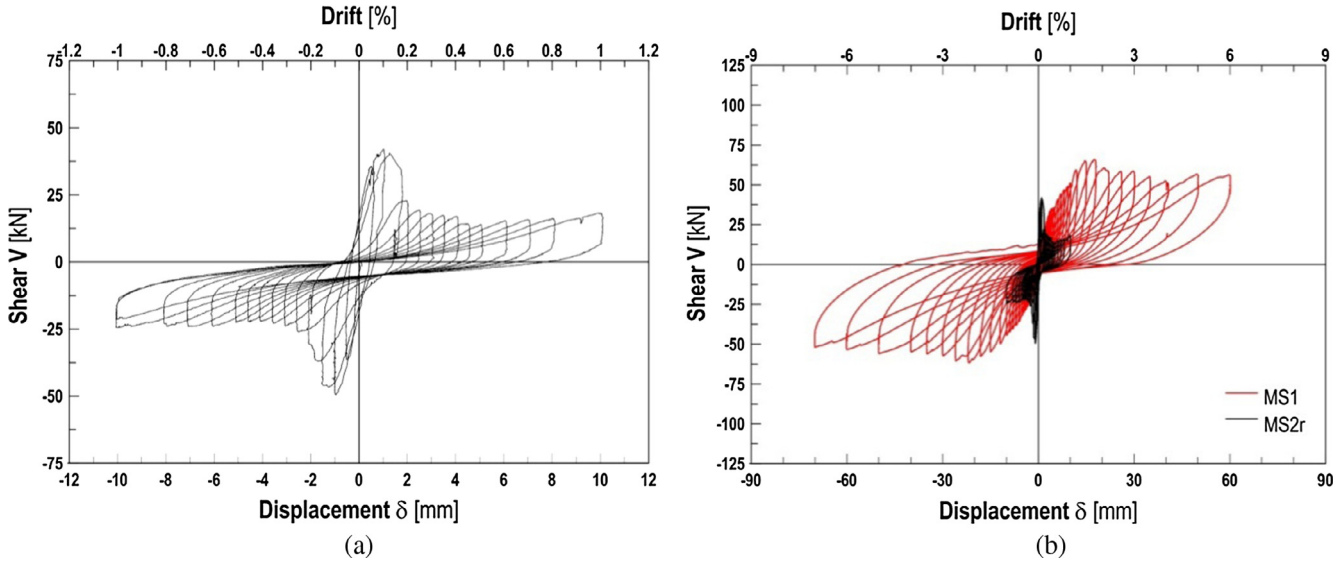

Fig. 6. MS2: shear load against vertical displacement (a); comparison of the behaviour of URM specimen MS2 and RM specimen MS2r (b).

positive and negative vertical displacements. In the former case a progressive reduction in shear capacity was observed; in the latter, the local debonding on CFRP laminates led to a rapid decrease of resistance. The increase in ductility was quite limited ranging from 2 (negative vertical displacement) and 3 (positive vertical displacement). The crack pattern was similar to that occurred in the URM specimen, but their opening was smaller, so that the axial load in the spandrel may be awaited to increase.

The relationship between the shear load and the relative vertical displacement of the unreinforced stone specimen MS4 is shown in Fig. 8a. In this test a maximum shear value of about 28 kN was obtained. Beyond the peak, the resistance remained almost constant up to a vertical displacement equal to about 0.8% of the spandrel length, when the test was terminated. The cracks surveyed in this test were vertical and were placed at the ends of the spandrel (flexural cracks).

The intervention adopted in this case is similar to that of sample MS2: the cracks were closed through a couple of temporary steel bars and an L-shaped steel profile ($100 \times 150 \times 15$ mm) was connected to the internal face of the wall at the floor level by means of dowels ($\Phi = 16$ mm) driven into the wall with a spacing of 500 mm and injected with thixotropic cement grout. The temporary bars were removed before starting the test. The graph of the shear load versus the relative vertical displacement of the MS4r sample is shown in Fig. 8b (red line), the black curve is that of the unreinforced specimen and it is reported for a direct comparison. The maximum resistance achieved by the specimen was about 60 kN, that is more than twice the resistance reached with the URM specimen MS4. After the peak load, the resistance remained almost constant up to a spandrel drift of 6%, and then it decreased slowly. The test was ended with a significant damage in correspondence of a spandrel drift of about 8%, nevertheless the residual resistance was from 60% to 85%. At this point, diagonal cracks were visible and the previously formed vertical cracks started to widen.

For each experimental test, the whole sequence of loading and unloading is displayed in the figures from 5–8. The main features of the experimental results are summarized in Table 2.

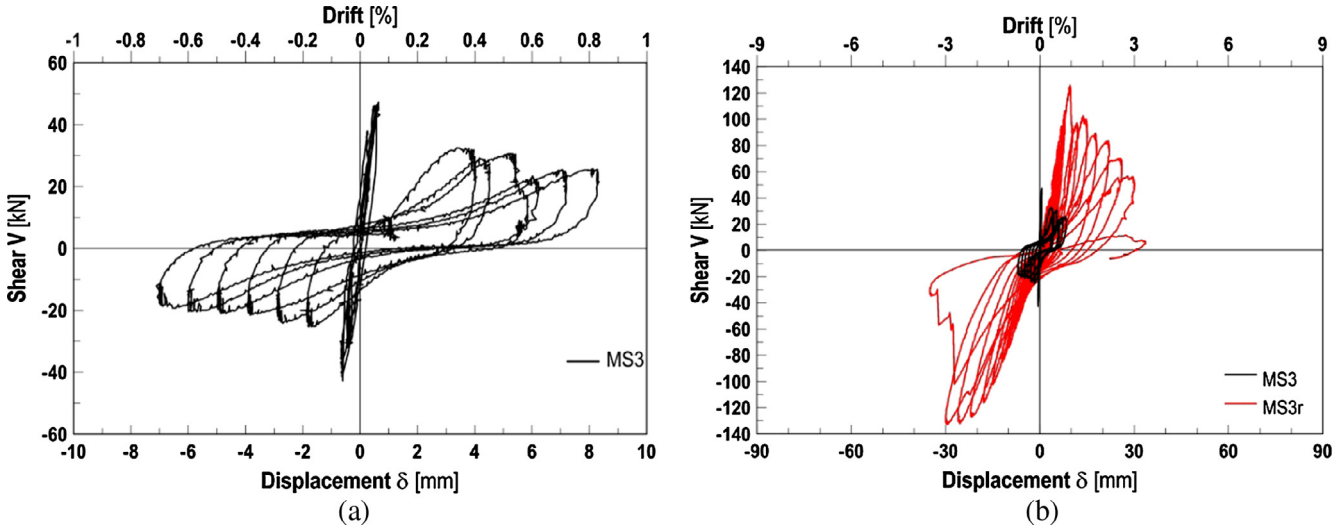

Fig. 7. MS3: shear load against vertical displacement (a); comparison of the behaviour of URM specimen MS3 and RM specimen MS3r (b).

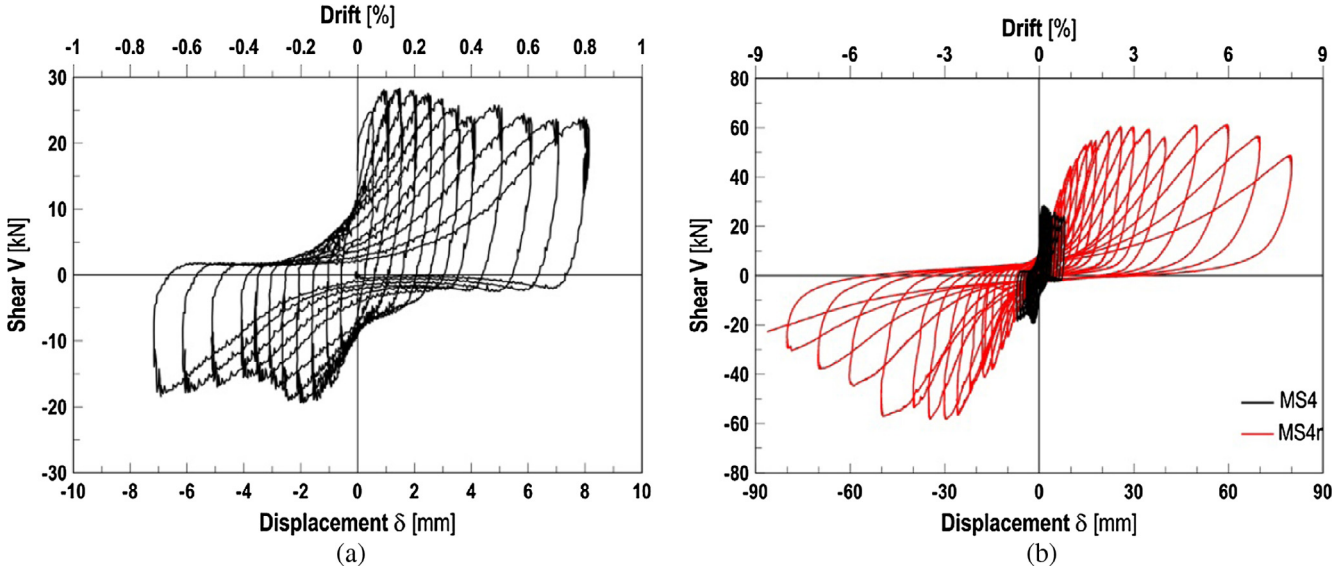

Fig. 8. MS4: shear load against vertical displacement (a); comparison of the behaviour of URM specimen MS4 and RM specimen MS4r (b).

Table 2
Summary of the experiment test results.

Specimen	Masonry type	Strengthening technique	Collapse mechanism	V_{max} [kN]	u_{ult} [mm]	Shear load at ultimate disp. [kN]
MS1	Clay bricks	None	Vertical cracks at both ends	70	10	38
MS1r	Clay bricks	Two horizontal steel ties	Diagonal cracks	95	72	50
MS2	Clay bricks	None	Diagonal cracks	50	10	19
MS2r	Clay bricks	Angle steel profile (100 × 200 × 10 mm)	Diagonal cracks	65	70	51
MS3	Clay bricks	None	Diagonal cracks	45	8	21
MS3r	Clay bricks	CFRP laminates	Diagonal cracks	130	31	10
MS4	Rubble stone	None	Vertical cracks at both ends	28	8	22
MS4r	Rubble stone	Angle steel profile (100 × 200 × 10 mm)	Diagonal cracks	60	80	45

In all the presented specimens (Figs. 5–8), it can be noticed how the initial stiffnesses in retrofitted specimens noticeably change from the unreinforced cases, due to the cracks developed.

Finally, the crack patterns obtained at the end of the test for the unreinforced specimens are depicted schematically in Fig. 9.

3. Mechanical modelling

The mechanical behaviour of a spandrel involves typically two types of failure: the flexural and shear collapse. The proposed relationships for each type of failure are presented afterwards.

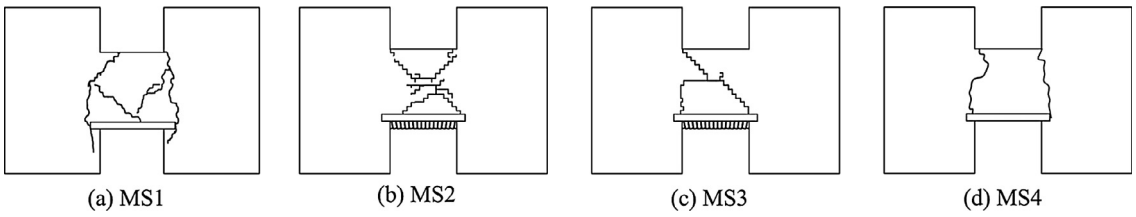

Fig. 9. Crack patterns developed at the test of unreinforced specimens (backward view).

Actually, in the last revision of the New Zealand guidelines for masonry assessment [24], an updated proposal for the flexural and shear resistance of URM spandrels, based mainly on the results reported in [4], is included. However, due to the very limited experimental research carried out on masonry spandrels [5,7,19], the relationships presented in the following were derived from the literature and modified and/or integrated on the basis of what was evidenced by experimental results.

3.1. Unreinforced spandrels

The code FEMA 306 [18] proposes the expression reported in Eq. (1) for estimating the flexural capacity in spandrels. The presented expression, valid for brick masonry, is related to the simple flexural strength of the un-cracked transversal section, and takes into account an equivalent tensile resistance due to interlocking at bed joints at the intersection between spandrel and piers (Fig. 10a),

$$M_{R1} = \frac{2}{3} \cdot f_{t,eq} \cdot t_s \cdot \frac{h^2}{4}, \tag{1}$$

where h represents the spandrel depth without lintel; t_s = spandrel thickness; with $f_{t,eq}$ the equivalent tensile resistance due to interlocking which is given by

$$f_{t,eq} = \frac{b_{eff}}{b_h} \cdot (f_{v0} + 0.65\,\sigma_p), \tag{2}$$

where f_{v0} is the initial shear strength of masonry in absence of axial force (cohesion); σ_p corresponds to the vertical compressive stress in the adjacent pier; b_{eff} is the effective interlocking length and b_h is the thickness of a brick plus a mortar joint (see Fig. 10a). The constant 0.65 is a reduction factor of compressive stress suggested by Cattari and Lagomarsino [17].

The shear resistance V_{R1} associated with the flexural capacity can be expressed with the relation

$$V_{R1} = \frac{2M_{R1}}{L}, \tag{3}$$

where L is the spandrel length.

For rubble stone masonry, the same Eq. (2) can be used, but assuming for f_{v0} a value equal to the shear strength obtained from diagonal compression tests f'_{v0} .

The second collapse mechanism accounted for in the FEMA 306 manual [18] is due by the occurrence of diagonal cracking. In this case, for a rectangular spandrel section, assuming a constant shear stress distribution, the shear resistance can be obtained as

$$V_{R2} = f_{tm} \cdot h \cdot t_s \cdot \delta \cdot \sqrt{1 + \frac{\sigma_h}{f_{tm}}} \quad with\ \delta = \frac{h}{L}\ and\ 0.67 \leqslant \delta \leqslant 1.0, \tag{4}$$

where σ_h is the horizontal stress (compression positive) normally equal to zero, f_{tm} is the tensile diagonal strength which, according to FEMA 273 [25], can be assumed equal to the cohesive strength of mortar bed joints f_{v0} and δ is the spandrel shape factor.

It has to be pointed out that the lintels used in the specimens tested give different contributions to the ultimate shear capacity of the unstrengthened spandrels, as evidenced by the experimental results. More specifically, the influence of the timber lintel is negligible for specimens MS1, MS4 because of its insignificant stiffness compared to that of the masonry part of the spandrel, which leads to very little stresses in the lintel before the occurrence of cracks in the masonry coupling beam. Differently, in specimens MS2 and MS3, the flat masonry arch at the bottom of the spandrel causes a horizontal thrust that is equilibrated by horizontal tensile forces in the masonry above, leading to a reduced spandrel shear capacity. Assuming that before cracking the shear force carried by the flat arch is proportional to its depth h_{arch}, the horizontal thrust due to diagonal struts developing in the flat arch can be calculated using equilibrium considerations as in CEN 2005 – Eurocode 6 [26] obtaining

$$H_{arch} = V \cdot \frac{L}{0.9 \cdot h_t}, \tag{5}$$

where H_{arch} is the horizontal thrust, V is the total vertical shear and h_t represents the spandrel depth with the lintel. The tensile stress in the masonry spandrel can then be calculated as

$$\sigma_h = \frac{H_{arch}}{t_s \cdot h}. \tag{6}$$

This has to be considered in the calculation of the shear resistance in Eq. (4), leading to a reduced shear resistance V_{R2}.

3.2. Reinforced spandrels

The spandrels were strengthened after completing the test on the plain condition. So that the reinforcing techniques were applied on cracked spandrels. The relationships used to assess the spandrel shear resistance are those provided by the Italian Code for Structural Design [31]. The first expression enables the consideration of the tensile resistance force H_p provided by the bars or the angle. In particular, H_p is equal to the axial resistance of the bars or, in the latter case, to the shear resistance of the dowels connecting the angle to the masonry piers. It is assumed that at failure the ultimate masonry compressive strength along the horizontal direction f_{hc} is reached at the compressed corners of the spandrel (diagonal strut). Thus using equilibrium, the shear resistance V_{R3} due to combined axial-bending failure can be calculated as

$$V_{R3} = \frac{H_p \cdot h}{l} \cdot \left(1 - \frac{H_p}{0.85 \cdot f_{hc} \cdot h \cdot t_s}\right) \quad with\ H_p \leqslant 0.4 \cdot f_{hc} \cdot h \cdot t_s \tag{7}$$

For the spandrel reinforced with CFRP laminates located at top and bottom of the spandrel, the value V_{R3} is derived from the resisting bending moment of the cross sections of the spandrel. The relationship can be easily derived using equilibrium

$$V_{R3} = \frac{H_C}{l} \cdot \left(2d + b_f - \frac{H_C}{0.85 \cdot f_{hc} \cdot t_s}\right) \quad with\ H_c \leqslant 0.4 \cdot f_{hc} \cdot h \cdot t_s, \tag{8}$$

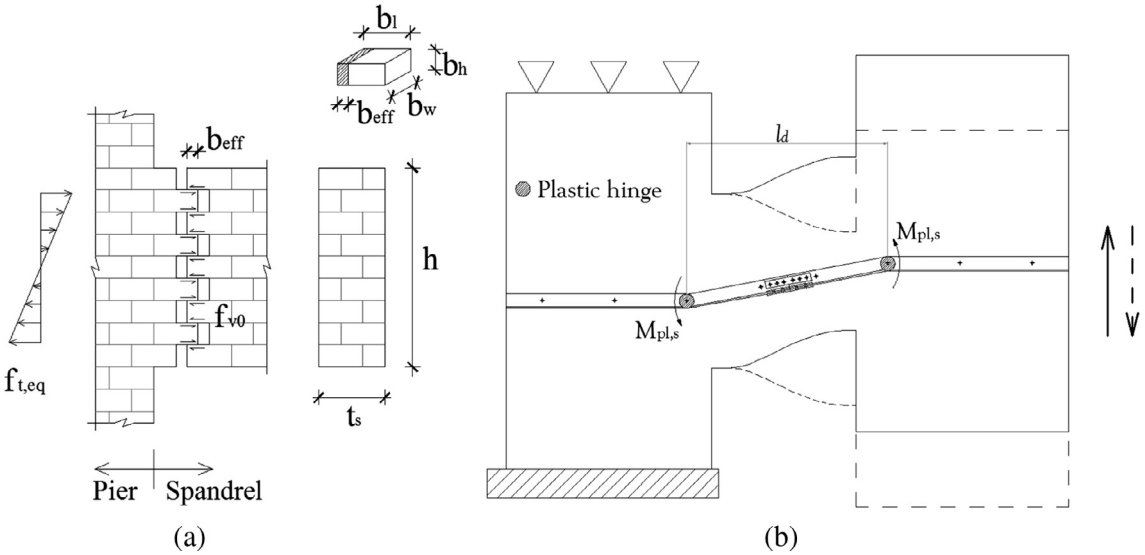

Fig. 10. Elastic stress distribution assumed at both ends of the masonry spandrel (a) and resisting mechanism for the specimen MS2r (b).

where d is the distance between top and bottom CFRP laminates, b_f is the laminate width and H_C is the maximum axial resistance of the couple of CFRP lamina at the top or at the bottom of the spandrel. This axial resistance correspond to the debonding resistance of the composite at adhesive-brick interface that is evaluated as

$$H_C = 2 \cdot f_{fd} \cdot b_f \cdot t_f, \tag{9}$$

in which t_f is the thickness of the composite laminate and f_{fd} is the tensile resistance considering the debonding. This resistance, according to the CNR-DT 200 R1/2013, is obtained through the relation

$$f_{fd} = \sqrt{\frac{2 \cdot \Gamma_d \cdot E_f}{t_f}}, \tag{10}$$

where E_f is the Young Modulus of the composite in the fibre direction and Γ_d is the specific fracture energy related to the debonding of the laminate. The fracture energy is given by the relation, expressed in Eq. (11):

$$\Gamma_d = k_b \cdot k_G \cdot \sqrt{f_{bm} \cdot f_{btm}}, \tag{11}$$

where k_b is a geometric coefficient, equal to 1 when the laminate has a width equal to the brick dimension, k_G is a coefficient depending on the material of the support, equal to 0.031 mm for brick masonry, f_{bm} and f_{btm} are the compressive and tensile strength of bricks. In the studied cases the optimal anchorage length is always guaranteed so that no reductions to the value of the tensile resistance obtained with Eq. (10) are necessary.

The second shear capacity model proposed by the Italian Code for Structural Design [31] due to the masonry considers shear sliding at vertical mortar joints along the diagonal direction. The shear resistance V'_{R4} depends upon the masonry initial shear strength f_{v0}, in the case of uncracked spandrels, and the compressive stress along the spandrel longitudinal axis σ_h, and it is given by

$$V'_{R4} = f_{vm} \cdot h \cdot t_s \quad with\ f_{vm} = f_{v0} + 0.4 \cdot \sigma_h. \tag{12}$$

This last contribution can be accounted to calculate the shear capacity of the strengthened specimens, as the cracks induced in the specimens in the first tests were closed by applying a tying force giving rise to horizontal compressive stresses in the spandrel of σ_h = 0.15 MPa. Actually this axial force is changing during test, but this variation is almost negligible up to reaching the peak shear load, as evidenced, for specimens MS1r, MS2r, by the values of the relative horizontal displacements of the piers, displayed in [7]. Similar results were also obtained for specimens MS3r and MS4r. So that the compressive horizontal stress σ_h used in Eq. (12) for all specimens was equal to 0.15 MPa.

For specimens MS1 and MS4, large cracks developed mainly at the ends of the spandrel [20,7], the contribution of the masonry spandrel to the shear capacity of the strengthened specimens MS1r, MS4r can be calculated using Eq. (12) accounting for both the cohesive and frictional contribution. Conversely, for specimens MS2 and MS3, as cracks developed mainly along the diagonal direction, the shear strength associated with the masonry shear strength with no compressive stresses should be neglected in Eq. (12) to calculate the shear capacity of the masonry part of the strengthened specimens MS2r and MS3r.

An additional resistance given by reinforcement has to be added to the shear strength: steel angle for specimens MS2r and MS4r and composite laminates for specimen MS3r. In the former, considering the development of plastic deformations in the steel angle (plastic moments) in correspondence of its connection to both piers (Fig. 10b), the following additional contribution to the shear capacity of specimens MS2r and MS4r is given by

$$V_{angle} = \frac{2 \cdot M_p}{l_d}, \tag{13}$$

where M_p is the plastic moment of the steel angle and l_d is the distance between plastic hinges. In the latter case, the shear resistance due to the composite laminates crossing the diagonal crack has to be considered. This resistance is the lesser between the tear off of the laminate and the debonding of the composite in a zone close to the crack. The experimental test evidenced the occurrence of the debonding of the laminate without any damage to the composite. The debonding resistance may be assessed considering the bond strength given by the relationship

$$f_b = \frac{2 \cdot \Gamma_d}{s_u}, \tag{14}$$

in which s_u is the value of the ultimate slip between the composite and the brick, assumed equal to 0.4 for brick masonry as proposed in CNR-DT 200 R1/2013 [27]. This bond strength is multiplied by an area equal to 0.75 b_f^2, as evidenced by experimental tests, so the shear resistance due to CFRP laminates is

$$V_{CFRP} = n \cdot f_b \cdot 0.75 \cdot b_f^2, \tag{15}$$

where n is the number of laminates crossing one diagonal crack (equal to 4 for specimens considered). The shear resistance of the reinforced spandrels related to the shear capacity is

$$V_{R4} = V'_{R4} + V_{angle} \quad or \quad V_{R4} = V'_{R4} + V_{CFRP}. \tag{16}$$

3.3. Strength by the proposed relationships

For all the considered tests, the shear resistance was calculated utilizing the equations described in the preceding sections, and the results are summarized in the Table 3. The values presented were used also in [7] to predict the strength of the specimens MS1, MS2 and their strengthening.

For URM and RM specimens, the previously presented relationships were employed, case by case depending on the reinforcement type.

For URM specimens, the relationships proposed predict the strength with a maximum error of 14.51%, while the difference with the experimental values from the reinforced specimens is lower than 20%.

In particular, in specimen MS1 the flexural capacity prior to cracking predicts accurately the spandrel behaviour. In the reinforced specimen MS1r, the maximum resistance was governed by a shear collapse of the spandrel with the formation of a diagonal crack, as occurred in the experimental test.

For test MS2, the shear capacity is dominant with respect to the flexural capacity, with the formation of diagonal cracks, as observed during the test. The resistance of the strengthened specimen MS2r was also characterized by the shear capacity of the spandrel due to friction at crack interface increased by the contribute of the plasticization of the steel profile. The distance between plastic hinges was assumed equal to 1380 mm, which corresponds with the relative distance between the first dowel in both piers. The test MS3 presents the same collapse mechanism as MS2. For reinforced spandrel MS3r, the resistance is governed by the shear capacity of the spandrel due to friction at crack interface increased with that offered by the composite laminates crossing the diagonal crack.

The stone specimen MS4, as specimen MS1 reached the maximum resistance when the bending strength at both ends of the spandrel were achieved, as obtained in the test with the formation of two almost vertical cracks. The strengthened specimen MS4r reached the collapse by shear with the formation of a diagonal crack. The resistance obtained considers also the contribute of the steel angle. The distance between plastic hinges was 2380 mm, because the first dowel in the piers were too close to the vertical cracks and then offered a negligible vertical restrain.

In general, the analytical predictions are in quite good agreement with the experimental results both for URM and RM spandrels so that they may be used to assess the maximum resistance V_{max} in the numerical model described in the next section.

4. Numerical modelling

A numerical model to accurately represent the cyclic behaviour of the masonry spandrel has been developed by implementing a non-linear spring element in the commercial FEM solver Abaqus. These springs connects two coincident nodes and returns to the solver force and stiffness corresponding to a given displacement. This model was previously developed for masonry piers in [28]. The element can represent the cyclic behaviour of a masonry spandrel using the hysteretic law proposed by Tomazevic and Lutman [29], as can be seen in Fig. 11.

This law is formed by a tri-linear backbone curve (segments $OABC$ in Fig. 11a) and a bilinear unloading/reloading path (segments bDb^* for unloading starting from branch AB, or $cD'c^*$ starting from BC; segments b^*D^*b for reloading starting from branch A^*B^*, or $c^*D'^*c'$ starting from B^*C^*).

This model takes into account linear stiffness degradation, involving the first unloading branch (bD and b^*D^* in Fig. 11a, which has a lower stiffness that elastic branch OA), and a strength degradation, which is proportional to dissipated energy. The stiffness degradation is linear, as can be seen in Fig. 11c, and involves the unloading branches bD and cD' (or b^*D^* and $c^*D'^*$ for reloading) in Fig. 11a; the unloading stiffness changes from the elastic value to a fully degraded stiffness K_u, that is used at the ultimate displacement, and defined through the parameter α:

$$K_u = \alpha K_{el}. \tag{17}$$

Moreover, the model includes also a strength degradation, which is introduced by an additional displacement (Δu in Fig. 11a) at the end of the reloading path. The strength degradation is proportional to the energy dissipated in a full cycle, indicated in Eq. (18) with ΔE_h:

$$\Delta u = \beta\left(\frac{\Delta E_h}{V_{\max}}\right). \tag{18}$$

The spring can be used in an equivalent frame modelling of a building and can be made connecting the spring, which is initially zero-length, to rigid beams as depicted in Fig. 11b. The spring needs 6 fundamental input parameters, such as:

- K_{el} elastic stiffness of the spandrel (slope of branches OA and OA^*);
- V_y shear strength of the spandrel at first cracking;
- K_{p1} first plastic stiffness of the spandrel (slope of branches AB and A^*B^*);
- V_{max} maximum shear strength of the spandrel;
- K_{p2} second plastic stiffness of the spandrel (slope of branches BC and B^*C^*);
- u_{ult} ultimate displacement of the spandrel.

In addition to these, three more parameters are needed to describe stiffness and strength degradation:

- γ defined in (0, 1), sets the percentage of unloading from the backbone curve for branches bD and cD' (or b^*D^* and $c^*D'^*$);
- α defined in (0, 1), sets the ultimate stiffness K_u through the relationship in Eq. (17);
- β defined in (0, 1), sets the strength degradation through the relationship in Eq. (18).

The parameter γ may be assumed equal to 0.6–0.9 according to the dissipative capacity of masonry type. The stiffness degradation parameter α can be assumed as 0.8, which means that the unloading stiffness immediately before failure is the 80% of the elastic one, while the strength degradation parameter β may be taken equal to 0.06, as suggested by Tomazevic and Lutman [29] after an experimental campaign on masonry piers, and as confirmed by Gattesco and Macorini [21]. The model, described completely in [28], is used also for masonry piers. The elastic stiffness of the spring is:

$$K_{el} = \frac{G \cdot A}{\chi \cdot l} \tag{19}$$

where G is the shear modulus, A is the sectional area of the spandrel, l is spandrel length, χ is the shear factor, always equal to 1.2 for rectangular sections.

The stiffness of the plastic branches (ABC and $A^*B^*C^*$ in Fig. 11a) are assumed as a percentage of the elastic stiffness. The slopes of

Table 3
Strength prediction from proposed relationships.

Specimen	MS1	MS1r	MS2	MS2r	MS3	MS3r	MS4	MS4r
f_{v0} [MPa]	0.19	0.19	0.22		0.19		0.10	0.10
f'_{v0} [MPa]							0.10	0.10
f_{hc} [MPa]		7.00		7.00		6.80		3.60
$f_{ys,D}$ [MPa]		950						
A_s [mm^2]		1145						
$f_{ys,b}$ [MPa]				480				480
Dowels				3M16				2M16
H_p [kN]		173.14		90.86				57.36
H_C [kN]						96.38		
σ_p [MPa]	0.5		0.5		0.5		0.5	
σ_h [MPa]		0.15		0.15		0.15		0.15
b_h [mm]	65	65	65	65	65	65		
b_{eff} [mm]	60	60	60	60	60	60		
t_s [mm]	380	380	380	380	380	380	400	400
h [mm]	1080	1080	980	980	980	980	1050	1050
h_t [mm]	1200	1200	1240	1240	1240	1240	1200	1200
d [mm]						760		
l_d [mm]				1380				2380
L [mm]	1000	1000	1050	1050	1050	1050	1000	1000
δ	1.08	1.08	0.93	0.93	0.93	0.93	1.10	1.10
Shear resistance								
V_{R1} [kN]	70.23		58.28		55.08		26.43	
V_{R2} [kN]	77.98		56.73		49.26		42.00	
V_{R3} [kN]		173.73		103.83		148.34		66.14
V_{R4} [kN]		102.60		53.02		120.38		59.79
V_{min} [kN]	70.23	102.60	56.73	53.02	49.26	120.38	26.43	59.79
V_{exp} [kN]	69.85	95.2	49.54	65.93	45.00	130.00	28.00	60.00
Diff.%	0.54%	7.77%	14.51%	−19.58%	9.47%	−7.40%	−5.61%	0%

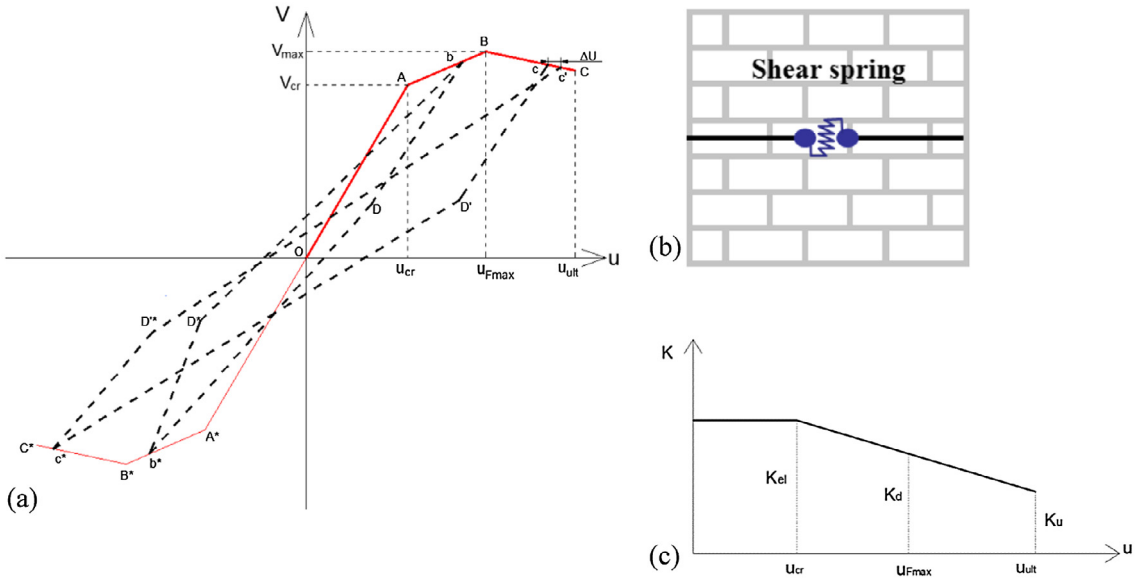

Fig. 11. Hysteretic rules proposed by Tomazevic and Lutman [29].

the plastic branches are calculated on the base of the strength at ultimate displacement and on a supplemental input parameter that specifies at which displacement the maximum strength occurs.

In addition, the shear strength of the spandrel at first cracking V_y may be assumed as a quote of the maximum shear strength V_{max}: a reasonable value for masonry spandrels may be 0.8, as suggested by experimental results. Finally, the ultimate displacement of the spandrel u_{ult} may be fixed according to some experimental or code indications (maximum drift). The values of the maximum resistance V_{max} used to define the springs characteristics were taken from the analytical results in Table 3.

The model built for the numerical simulation uses the equivalent frame method [30] to schematize the experimental setup; the nodal regions are hence modelled with rigid links. The resulting model employs Euler-Bernoulli (EB.) beams for the spandrel, since the Timoshenko's shear contribution is accounted in the spring elements (Eq. (13)), and beams with the Timoshenko shear stiffness contribution for the piers (Fig. 12). The previously described shear spring is placed in the middle of the spandrel. The whole scheme is simply supported in the lower left and the upper right corner; these supports include a bi-linear elastic rotational spring which represents, in a lumped way, the contact of the pier end with the test apparatus.

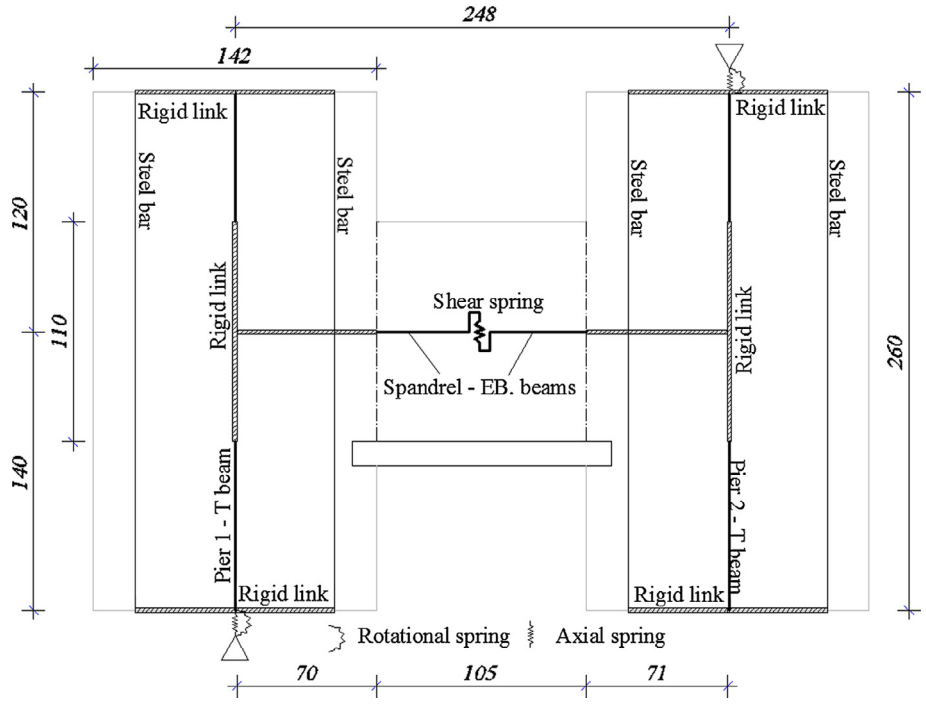

Fig. 12. Equivalent frame model adopted for the numerical simulations, units in cm.

The rotational springs in Fig. 12 were calibrated via a simple additional model involving the single pier depicted in Fig. 13a, which enabled to get the moment-rotation law for the springs. The pier has been modelled with shell elements and rigid links at the top and in the middle height, placed respectively to simulate the real external boundary conditions and to apply the moment M caused by the spandrel shear in the middle of the pier. The elastic moduli employed for the isotropic materials in this simulation are 4800 MPa for the brick masonry [7], 2500 MPa for the stone masonry and 210,000 MPa for the Dywidag bars.

The pier is supported at the base with compression-only springs to allow the uplift; they have been characterized with a bilinear law with a numerically high stiffness in compression and a null one in tension. Moreover, the Dywidag bars were modelled with trusses reacting in tension only. A first non-linear static analysis has been performed with a thermal load of −77 °C on the bars (which have a coefficient of thermal expansion of 1.17e−5 1/°C), in order to induce the experimental compression of 0.5 MPa in the piers. Hence, a second non-linear static analysis were performed applying simultaneously with a ramp the force F and the moment M depicted in Fig. 13a.

The model allowed to obtain the moment-rotation law shown in Fig. 13b, measured at the base of the panel, which has been introduced as a bi-linear elastic law in the flexural springs in the scheme depicted in Fig. 12.

Finally, all the experimental tests have been simulated applying the test displacement to the right-hand pier. The parameter γ was assumed equal to 0.7, for solid brick masonry, and equal to 90% for rubble stone masonry. In fact, as evidenced by experimental tests, a larger energy dissipation at each cycle was evidenced in rubble stone spandrel because of the significant interlocking effect at crack interface due to the irregularity of mortar joints with respect to those of solid brick (regular horizontal joints).

Elastic stiffness was calculated for each test with Eq. (13) for the unreinforced specimens, while for the reinforced specimens, for which the transversal section is cracked, the 10% of the initial un-cracked stiffness has been assumed, averaging the values obtained from the tests. The post-elastic stiffnesses for the backbone curve are suggested in [29]: are 9.1% and −4.8% the elastic stiffness; the authors however preferred to adopt only the first suggested value and then connect the point with the maximum strength to the point (u_{ult}, V_{res}) – ultimate displacement and residual strength obtained experimentally. In such a way, the effects of any post-peak axial load variation (Section 3.2) are implicitly included in the softening slope employed. In particular, the residual strength varies between 40% and 50% the maximum one for solid brick masonry, and 75% for rubble stone masonry, when no reinforcements were applied. For spandrels strengthened with steel bars or angles, the residual strength was assumed between 50% and 75% the maximum one and equal to 50%, for spandrels strengthened with CFRP strips.

The maximum shear strength was derived through the equations reported in Section 3. The ultimate displacements were estimated using 0.8% and 6% of the spandrel length for the unreinforced and reinforced cases respectively. Actually, for the specimen reinforced with CFRP strips, a lower ultimate displacement was used (u_{ult} = 2.8%), as obtained in the experimental test. These ultimate displacements are not conservative for design purposes, but allow performing the simulation until the end of test protocols. The comparison between experimental and numerical cycles is reported in figures from 14–17.

The results show a good agreement of numerical cycles with experimental results. Provided the accuracy in cyclic field, this model can be used to estimate the dissipative capacity of masonry spandrels. It can be observed that the energy dissipation increases with the amplitude of imposed displacement; moreover, the total energy for each simulation has been compared with the experimental values in Fig. 18.

It is in progress a study aimed to generalize the numerical model defining the softening branch B–C of the shear-displacement curve in Fig. 11 with an analytical relationship

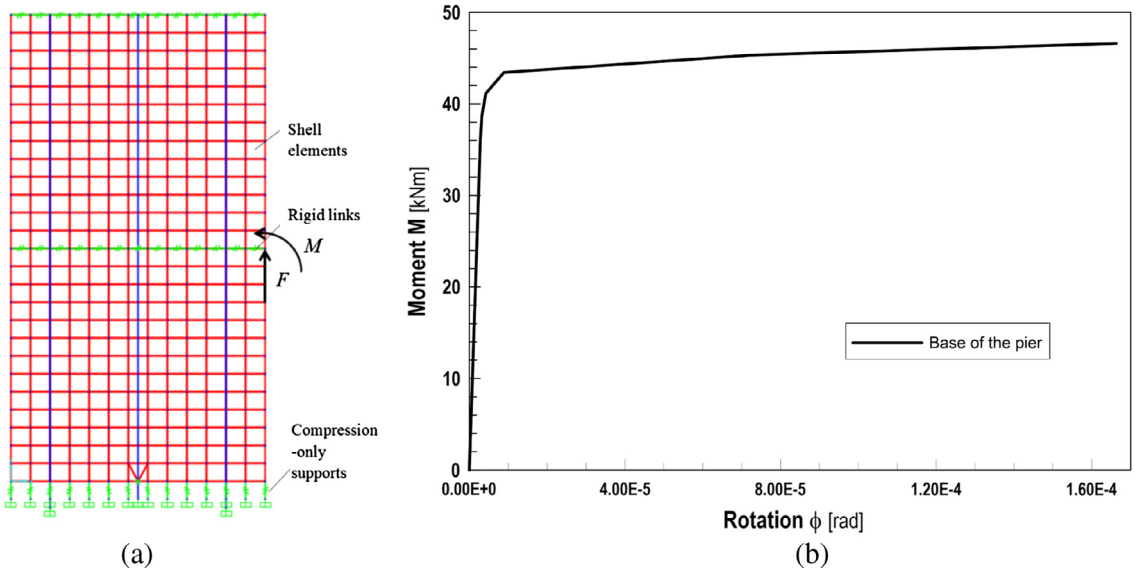

Fig. 13. Numerical model of the single pier (a) and moment-rotation law measured at the base (b).

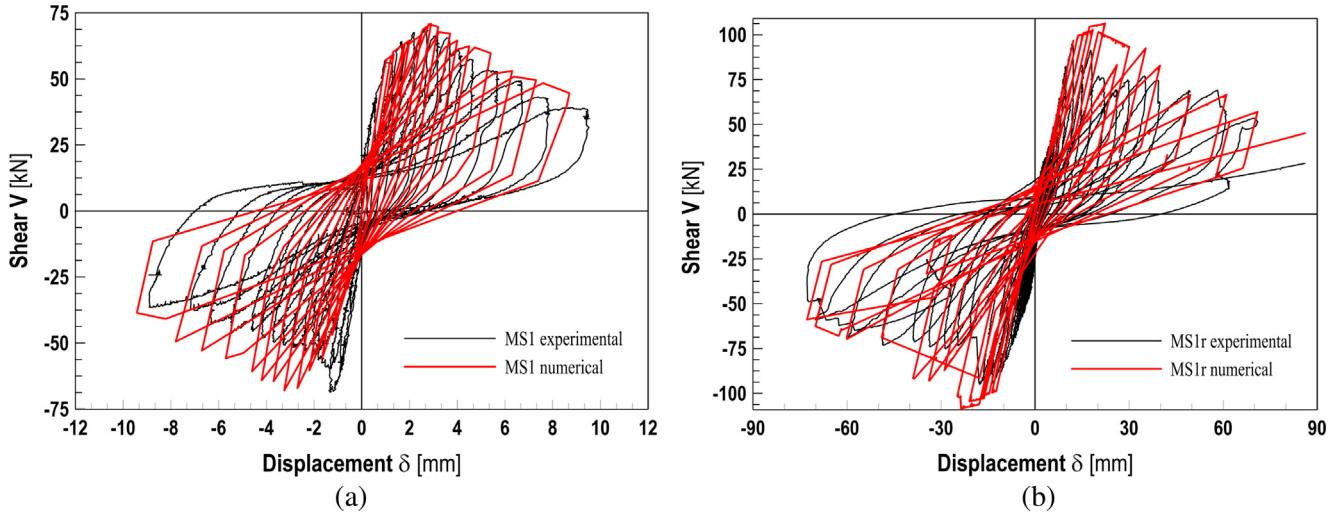

Fig. 14. Experimental-numerical comparison of MS1 (a) and MS1r (b) test results.

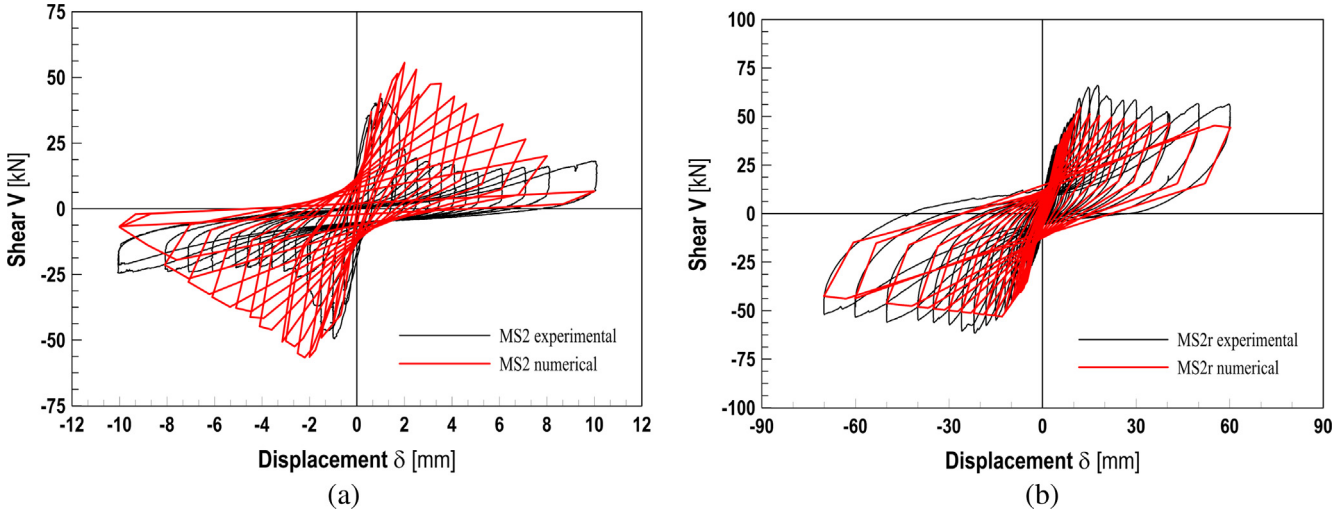

Fig. 15. Experimental-numerical comparison of MS2 (a) and MS2r (b) test results.

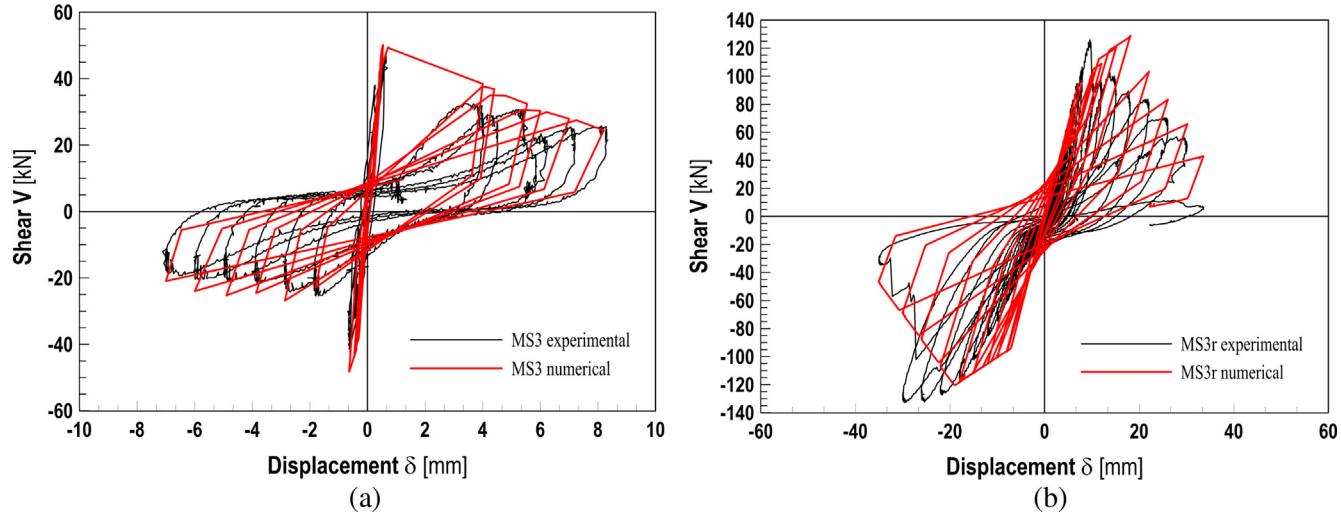

Fig. 16. Experimental-numerical comparison of MS3 (a) and MS3r (b) test results.

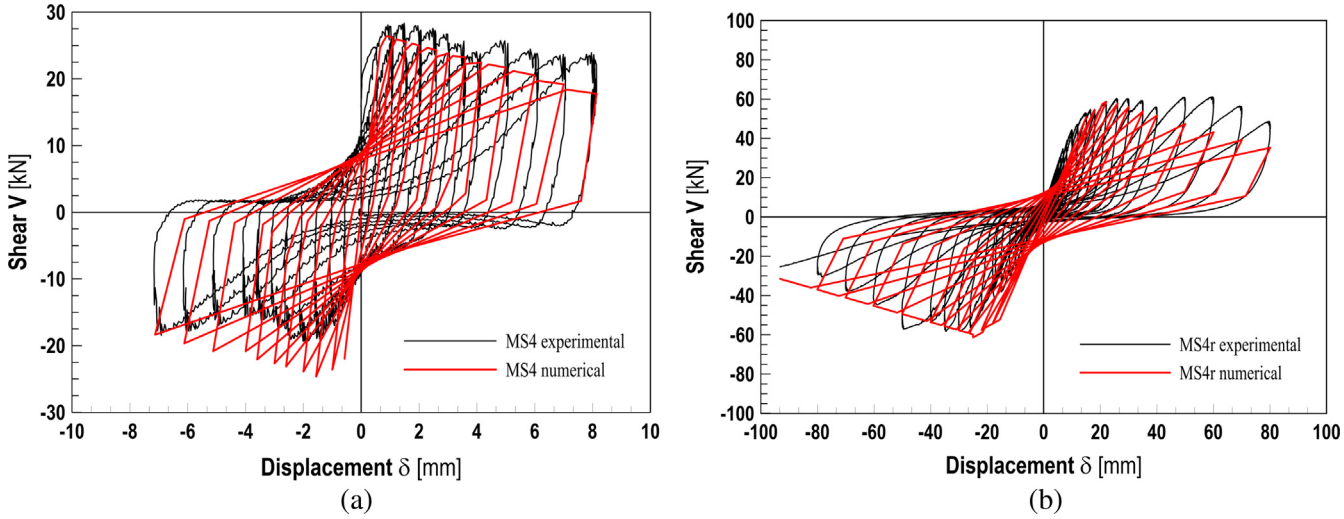

Fig. 17. Experimental-numerical comparison of MS4 (a) and MS4r (b) test results.

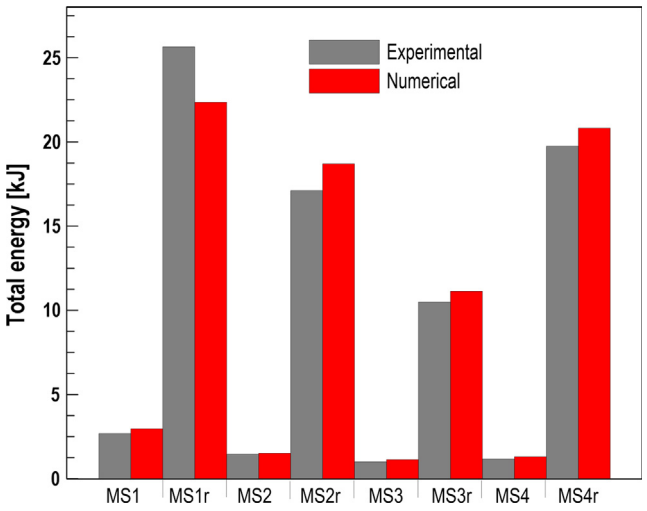

Fig. 18. Final values of the total energy calculated for each specimen (grey bars) and comparison with the numerical simulation (red bars). (For interpretation of the references to color in this figure legend, the reader is referred to the web version of this article.)

Table 4
Numerical/experimental differences in total energy.

Specimen	E_{num} [kJ]	E_{exp} [kJ]	Diff.%
MS1	2.96	2.69	10.14%
MS1r	22.35	25.64	−12.86%
MS2	1.51	1.45	4.35%
MS2r	18.70	17.11	9.33%
MS3	1.13	1.00	12.76%
MS3r	11.13	10.50	5.98%
MS4	1.31	1.17	11.65%
MS4r	20.82	19.74	5.46%

calibrated on the base of all the experimental results on masonry spandrels available in the literature [3,7,33].

As can be seen in Table 4, the maximum difference between experimental and numerical total energy at the end of the test is 13%.

5. Conclusions

An experimental campaign on cyclic behaviour of brick and stone masonry spandrels was conducted on 4 full-scale H-shape

unreinforced specimens. Each spandrel was subjected to shear by moving up and down one pier. All the tests have been conducted cyclically in displacement control. After a first test on the unreinforced specimen, each specimen was reinforced with several strengthening techniques such as steel rods (MS1r), steel angle (MS2r and MS4r) and CFRP laminates (MS3r).

The collapse mechanisms were studied and suitable relationships to calculate analytically the maximum strength were proposed for URM and RM spandrels and underlining all the contributions by the different resisting mechanisms. All the proposed relationships refer to well-known mechanism, as already outlined by FEMA 306 [18] and the Italian regulations [31]. A good agreement was obtained between the predicted resistance and the experimental strength for all the specimens, both strengthened and plain.

For the unreinforced specimens, the minimum strength provided by the sliding and the bending cracking mechanisms were considered, leading to predictions having a variation from the experimental values of a maximum of 15%. For the strengthened spandrels, the mechanism considered are related to the post-cracking behaviour, accounting for the tensile strength given by reinforcements, the shear contribution due to the plasticization of the steel profile and finally the contribution of the CFRP laminates by means of the relationships proposed by CNR-DT 200 [27]. The predictions in this case lead to a difference from the experimental results normally less than 10%, in only one case the difference approaches 20%.

A numerical approach based on lumped plasticity to approximate the experimental behaviour was developed and presented. This model, which starts from the Tomazevic and Lutman's proposal of the shear hysteretic rule [29], is able to predict the cyclic response of a masonry spandrel and to predict the dissipated energy during cycles. The proper static scheme has been applied, with particular attention to the boundary conditions: the tests were reproduced using the equivalent frame method and considering the stiffnesses introduced by the H-shape specimen in the spandrel response. Static cyclic analyses, performed for each specimen, led to a good agreement with experimental results, measured in terms of total energy at the end of the test, with a maximum difference less than 13%.

Finally, the analytical predictions reported in this paper have been validated through specific tests and they gave a good prediction of the spandrel capacity. More tests are required to make a proposal for the newer version of design codes. Actually, none of the considered codes consider all the mechanism investigated.

This study can be further developed to the seismic vulnerability evaluation of masonry buildings, with particular attention to spandrel behaviour, which are often neglected in evaluating the building capacity. The presented numerical tool can be used also in dynamic analyses, permitting to take into account the real dissipative capacity of unreinforced and reinforced masonry spandrels. The beam elements and the spring can also be included in a macro-element, as it has been done in [32]. A study in progress is aimed to provide more generality to the numerical model defining the post peak shear-displacement branch with an analytical relationship calibrated upon the experimental results on masonry spandrels available in the literature (e.g. [3,7,33]).

References

[1] Bruneau M. State-of-art report on seismic performance of unreinforced masonry buildings. J Struct Eng ASCE 1994;120(1):230–51.

[2] Tomaževic M. Earthquake-resistant design of masonry structures. In: Elnashai AS, Dowling PJ, editors. Series on innovation in structures and construction, vol. 1. London UK: Imperial College Press; 2000.

[3] Gattesco N, Macorini L, Clemente I, Noé S. Experimental investigation on the behaviour of spandrels in ancient masonry buildings. In: 14th World conference on earthquake engineering, Beijing, China.

[4] Beyer K. Peak and residual strengths of brick masonry spandrels. Eng Struct 2012;41:533–47. http://dx.doi.org/10.1016/j.engstruct.2012.03.015.

[5] Beyer K, Dazio A. Quasi-static cyclic tests on masonry spandrels. Earthq Spectra 2012;28(3):907–29.

[6] Parisi F, Augenti N, Prota A. The role of spandrels within masonry walls with openings: and experimental investigation. In: Proceedings of the ninth Pacific conference on earthquake engineering, building an earthquake-resilient society, Auckland, New Zealand.

[7] Gattesco N, Macorini L, Dudine A. Experimental response of Brick-Masonry spandrels under in-plane cyclic loading. J Struct Eng 2015. http://dx.doi.org/10.1061/(ASCE)ST.1943-541X.0001418. ASCE.

[8] Beyer K, Mangalathu S. Numerical study on the peak strength of masonry spandrels with arches. J Earthq Eng 2014;18:169–86. http://dx.doi.org/10.1080/13632469.2013.851047.

[9] Beyer K, Mangalathu S. Review of strength models for masonry spandrels. Bull Earthq Eng 2012;11:521–42. http://dx.doi.org/10.1007/s10518-012-9394-3.

[10] FEMA 356. Prestandard for the seismic rehabilitation of existing structures. Washington DC: FEMA; 2000.

[11] Lourenço PB. Computational strategy for masonry structures PhD Thesis. Delft, The Netherlands: Delft University of Technology; 1996.

[12] EN 1998. Eurocode 8–design of Structures for earthquake resistance–Part 1: general rules, seismic actions and rules for buildings. European Standard NF EN, 1.

[13] Magenes G. A method for pushover analysis in seismic assessment of masonry buildings. In: 12th World conference on earthquake engineering, Auckland, New Zealand.

[14] Lagomarsino S, Penna A, Galasco A, Cattari S. TREMURI program: an equivalent frame model for the nonlinear seismic analysis of masonry buildings. Eng Struct 2013;56:1787–99. http://dx.doi.org/10.1016/j.engstruct.2013.08.002.

[15] Penna A, Lagomarsino S, Galasco A. A nonlinear macroelement model for the seismic analysis of masonry buildings. Earthq Eng Struct Dyn 2013;43:159–79. http://dx.doi.org/10.1002/eqe.

[16] Chen SY, Moon FL, Yi T. A macroelement for the nonlinear analysis of in-plane unreinforced masonry piers. Eng Struct 2008;30(8):2242–52.

[17] Cattari S, Lagomarsino S. A strength criterion for the flexural behaviour of spandrels in un-reinforced masonry walls. In: 14th WCEE world conference on earthquake engineering, China.

[18] ATC. FEMA 306 – Evaluation of earthquake damaged concrete and masonry wall buildings – basic procedures manual. Washington, D.C.; 1999.

[19] Graziotti F, Magenes G, Penna A. Experimental cyclic behaviour of stone masonry spandrels. In: Proceedings of 15th world conference on earthquake engineering, WCEE, Lisbon, Portugal.

[20] Amadio C, Gattesco N, Dudine A, Franceschinis R, Rinaldin G. Structural performance of spandrels in stone masonry buildings. In: 15th World conference on earthquake engineering, WCEE, Lisbon, Portugal.

[21] Gattesco N, Macorini L. In-plane stiffening techniques with nail plates or CFRP strips for timber floors in historical masonry buildings. Constr Build Mater 2014;58:64–76.

[22] Gattesco N, Boem I, Dudine A. Diagonal compression tests on masonry walls strengthened with a GFRP mesh reinforced mortar coating. Bull Earthq Eng 2014;13(6):1703–26.

[23] Gattesco N, Amadio C, Bedon C. Experimental and numerical study on the shear behavior of stone masonry walls strengthened with GFRP reinforced mortar coating and steel-cord reinforced repointing. Eng Struct 2015;90:143–57.

[24] NZSEE. Assessment and improvement of the structural performance of buildings in earthquakes. Study group on earthquake risk building, corrigenda 4, 9th April 2015. <http://www.nzsee.org.nz/publications/assessment-and-improvement-of-the-structural-performance-of-buildings-in-earthquake/>.

[25] ATC. NEHRP guidelines for the seismic rehabilitation of buildings and NEHRP commentary on the guidelines for the seismic rehabilitation of buildings. Prepared for the Building Seismic Safety Council. Washington, DC: FEMA; 1997.

[26] CEN. Eurocode 6: design of masonry structures—Part 1-1: common rules for reinforced and unreinforced masonry structures. EN 1996-1-1:2005, Brussels.

[27] CNR. CNR-DT 200 – Istruzioni per la progettazione, l'esecuzione e il controllo di interventi di consolidamento statico mediante l'utilizzo di compositi fibrorinforzati – Italian code; 2004 [in Italian].

[28] Rinaldin G, Amadio C, Macorini L. A macro-model with nonlinear springs for seismic analysis of URM buildings. Earthq Eng Struct Dyn 2016. http://dx.doi.org/10.1002/eqe.2759. Wiley Online Library (wileyonlinelibrary.com).

[29] Tomazevic M, Lutman M. Seismic behavior of masonry walls – modeling of hysteretic rules. J Struct Eng 1996.

[30] Kwan AKH. Analysis of coupled wall/frame structures by frame method with shear deformation allowed. Proc Instn Civ Engrs, Part 2 1991;291 (June):273–97.

[31] Italian Ministry of Infrastructure. Italian code for structural design (Norme Tecniche per le Costruzioni – NTC) (2008). D.M. 14/1/2008, Official bulletin no. 29 of February 4 2008 [in Italian].

[32] Rinaldin G, Amadio C. A macroelement for the cyclic analysis of masonry structures. In: Proceedings of CIVIL-COMP 2015 the fifteenth international conference on civil, structural and environmental engineering computing, Prague, Czech Republic, 1–4 September 2015, ISBN 978-1-905088-63-8. Paper 4.77 from CCP: 108.

[33] Augenti N, Graziotti F, Magenes G, Parisi F. Experimental researches on the seismic behaviour of masonry spandrels: an international perspective. Pavia: EUCENTRE Press; 2016, ISBN 978-88-6198-124-9.